Journal of Molecular Structure 1294 (2023) 136418

Contents lists available at ScienceDirect

Journal of Molecular Structure

journal homepage: www.elsevier.com/locate/molstr

A cucurbit[8]uril-based fluorescent probe for the selective detection of pymetrozine

Pei-Hui Shan [a], Ding-Wu Pan [a,*], Li-Xia Chen [a], Timothy J. Prior [b], Carl Redshaw [b,*], Zhu Tao [a], Xin Xiao [a,*]

[a] Key Laboratory of Macrocyclic and Supramolecular Chemistry of Guizhou Province, Guizhou University, Guiyang 550025, China
[b] Chemistry, School of Natural Sciences, University of Hull, Hull HU6 7RX, U.K.

ARTICLE INFO

Keywords:
Cucurbit[n]uril
Supramolecular assembly
Selective recognition
Fluorescent probe
Host–guest chemistry

ABSTRACT

Herein, we report a simple fluorescence-enhanced system for the selective recognition and determination of the insecticide pymetrozine. ^{1}H NMR spectroscopic data indicate that 1,2-bis(4-pyridyl)ethylene (BPE) is partially encapsulated in the cavity of the cucurbit[8]uril (Q[8]) in aqueous solution, forming a stable 1:2 host-guest inclusion complex. Good evidence is also provided by other characterization techniques including single crystal X-ray diffraction, UV–Vis and fluorescence spectroscopies. This host-guest inclusion complex shows weak fluorescence in aqueous solution. Interestingly, the addition of pymetrozine greatly enhanced the fluorescence of the host-guest inclusion complex. In contrast, no significant fluorescence enhancement was observed on addition of 10 other pesticides. The concentration of pymetrozine in aqueous solution was easily detected based on the linear relationship between fluorescence intensity and pymetrozine concentration. Therefore, this paper reports a new method to identify and determine pymetrozine by fluorescence enhancement.

1. Introduction

Cucurbit[*n*]urils (n=5–8,10,13–15, abbreviated as Q[*n*]s, Fig. 1) are composed of 2n methylene-bridged n-hydroxyurea units with a negatively charged portal hydroxyl oxygen and a positively charged outer surface structure [1–3]. Q[*n*]s are a relatively new class of macrocyclic hosts, which when compared to other macrocyclic moieties such as cyclodextrins, calixarenes and pillararenes, exhibit excellent properties in aqueous solution. Indeed, previous studies have shown that cucurbit[*n*]urils can bind to a variety of guests in aqueous solution, including organic molecules, metal ions, amino acids, peptides and a number of pesticides [4–16]. Q[*n*]s have found many applications in areas such as molecular recognition, [17–20] supramolecular polymers, [21–24] supramolecular hydrogels, [25,26] supramolecular organic frameworks [27–31] and adsorbing and separating materials [32–35].

The structure of the 1,2-bis(4-pyridyl)ethylene molecule (BPE) is characterized by the presence of an unsaturated group C=C, which allows it to undergo *cis-trans* photoisomerization [36]. Secondly, the presence of nitrogen atoms at both ends of the molecule can act as a "bridge" between two metal complexes or other structural units [37]. Given its structural properties, BPE is often used as a raw material for synthesis, as a catalyst for a particular reaction, and for the construction of metal-organic frameworks (MOF), solid coordination frameworks (SOF), polymers, clusters, etc. [38–45]. BPE does not show intrinsic fluorescence in aqueous solutions, however, when BPE interacts with Q[8], the resulting host-guest complexes weakly fluoresce. Although there are many reports of interactions by BPE and Q[*n*]s, there appear to be few reports relating to the detection of pesticides utilizing host-guest interactions. Based on this, we decided to investigate whether BPE can be encapsulated within the cavity of Q[8] to form an inclusion complex and whether the resulting BPE_2@Q[8] can be employed for the detection of pesticides. We note that in the case of paraquat, a review has recently appeared describing the various analytical techniques employed for its determination [46].

In this study, the binding properties of Q[8] with BPE were investigated using a variety of techniques including ^{1}H NMR, UV–Vis and fluorescence spectroscopies, single crystal X-ray diffraction techniques and isothermal titration calorimetry (ITC). The results revealed the formation of a 1:2 host-guest inclusion complex which exhibited weak fluorescence. More importantly, when pymetrozine (Fig. 1) was added to the 1:2 host-guest inclusion complex of BPE_2@Q[8], the fluorescence intensity of the inclusion complex was greatly enhanced. However, no

* Corresponding authors.
E-mail addresses: dwpan@gzu.edu.cn (D.-W. Pan), c.redshaw@hull.ac.uk (C. Redshaw), xxiao@gzu.edu.cn (X. Xiao).

https://doi.org/10.1016/j.molstruc.2023.136418
Received 24 April 2023; Received in revised form 7 August 2023; Accepted 12 August 2023
Available online 14 August 2023

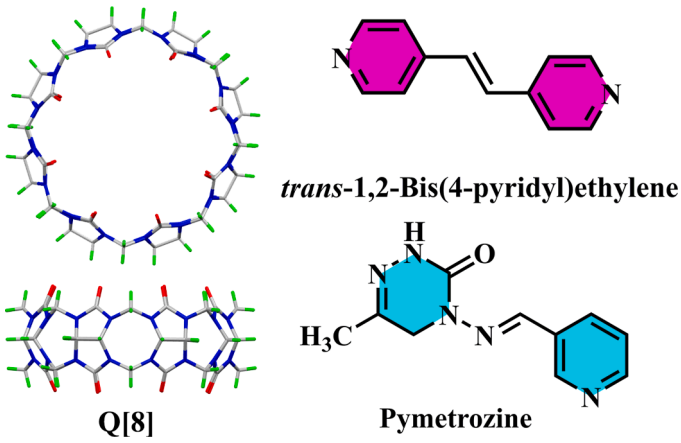

Fig. 1. The molecular structures of Q[8], BPE and Pymetrozine.

significant fluorescence enhancement was observed when any of the other 10 pesticides (methomyl, tricyclazole, praziquantel, carbendazim, paraquat, pyrimethanil, butachlor, thiamethoxam, acetamiprid, metoxazon; for the structures of the pesticides see Fig. S1 in the supplementary material) were added to the same inclusion complex. These observations suggest that the system can be used for the selective detection and determination of pymetrozine in aqueous solutions.

2. Experimental Section

2.1. Materials

Q[8] used in the experiments was prepared according to the literature method [47]. BPE and the pesticides were purchased from Aladdin (Shanghai, China). All other reagents used were of analytical grade and were used without further purification. Double-distilled water was used throughout the experiments.

2.2. Measurement of absorption, mass and fluorescence spectra

UV–visible spectroscopy was performed using an Agilent 8453 spectrophotometer (Agilent Technologies, Santa Clara, CA, USA) at ambient temperature. The fluorescence spectra were obtained using a Varian RF-540 fluorescence spectrophotometer. Stock solutions of Q[8] (1.00×10^{-4} mol·L^{-1}), *trans*-1,2-bis(4-pyridyl)ethylene (BPE,1.00×10^{-3} mol·L^{-1}) and all pesticides (2.00×10^{-2} mol·L^{-1}) were prepared using doubly-distilled water. A solution of the required concentration for the test was obtained by diluting the stock solution. For characterization by fluorescence emission spectroscopy, aqueous solutions of the BPE_2@Q[8] complex (BPE: 2.00×10^{-5} mol·L^{-1}) were prepared. Known concentrations of pesticides were added to the BPE_2@Q[8] complex to obtain the fluorescence spectra. The fluorescence spectra were obtained by excitation at 296 nm with an emission and excitation bandwidth of 5 nm, and the emission intensity was monitored at 478 nm at room temperature. The maximum emission wavelength was found to be λ_{em} = 478 nm for the BPE_2@Q[8] complex. To obtain the titration fluorescence spectra, pymetrozine (3.0, 6.0...60.0 μL, 2.00×10^{-2} mol·L^{-1}) was added to the BPE_2@Q[8] complex (3 ml 2.00×10^{-5} mol·L^{-1}) in quartz cells.

2.3. ^{1}H NMR measurements

All NMR spectroscopic data were recorded on a JEOL JNMECZ400s spectrometer in D_2O at 293.15 K. The observed chemical shifts are given in parts per million (ppm) relative to that of the internal tetramethylsilane (TMS) standard (0.0 ppm). ^{1}H NMR spectroscopic experiments were conducted using a Q[8] concentration of 5.0 × 10$^-$4 mol/L.

2.4. Crystallization and structure determination

A Bruker D8 VENTURE diffractometer employing graphite monochromatic Mo-*K*α radiation (λ = 0.71073 Å) at 200(2) K was used to collect the data. Empirical absorption corrections were applied by using the multiscan program SADABS. Structural solution and full matrix least-squares refinement based on F^2 were performed with the SHELXL-2018 and Olex2 packages [48–49]. Anisotropical thermal parameters were applied to all non-hydrogen atoms. Hydrogen atoms were treated as riding atoms with an isotropic displacement parameter equal to 1.2 times that of the parent atom. The SQUEEZE was used due to the presence of disordered solvent water molecules [50]. CCDC 2243977 contains the supplementary crystallographic data for this paper. These data can be obtained free of charge from The Cambridge Crystallographic Data Centre via www.ccdc.cam.ac.uk/data_request/cif.

2.5. Preparation of the complex

To a solution of *trans*-1,2-bis(4-pyridyl)ethylene (10.0 mg, 0.05 mmol) in 6 M HCl solution (2.5 ml) was added Q[8] (15.08 mg, 0.010 mmol). The mixture was stirred for 10 min at 60 °C and then filtered off. The filtrate was allowed to evaporate slowly (about 15 days) in air. Colourless crystals in the form of rhombic blocks of the complex were obtained. The data suggest that the guest *trans*-1,2-bis(4-pyridyl) ethylene is partially encapsulated in the cavity of the host Q[8], both in aqueous solution and in the solid state. This forms a highly stable inclusion complex.

3. Results and Discussion

3.1. Formation of the 1:2 inclusion complex in aqueous solution

To investigate the binding properties of Q[8] to BPE in aqueous solution, ^{1}H NMR spectroscopic titration experiments were carried out. The ^{1}H NMR spectroscopic data for BPE in neutral D_2O solution in the absence and presence of different equivalents of Q[8] is shown in Fig. 2. The continuous addition of Q[8] caused a significant upfield shift of the guest BPE Ha, Hb and Hc protons. The fact that the pyridine ring, as well as the double bond, is encapsulated within the cavity of the host can be used to rationalise this behaviour.

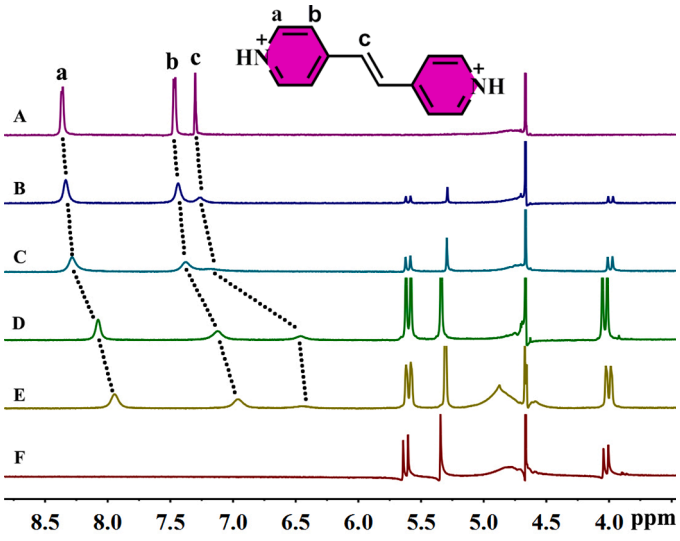

Fig. 2. . 1HNMR spectra of BPE (2.0 mmol/L) (A) in the absence of Q[8]; (B) with 0.23 equiv. of Q[8]; (C) with 0.53 equiv. of Q[8]; (D) with 0.78 equiv. of Q[8]; (E) with 1.05 equiv. of Q[8]; (F) neat Q[8] in D_2O at 20 °C.

3.2. UV–vis and fluorescence spectroscopy

UV–Vis (Fig. 3) and fluorescence (Fig. 4) spectroscopic titration experiments were carried out to further investigate the binding properties of Q[8] toward BPE in aqueous solution. BPE exhibits a characteristic absorption peak at 310 nm as shown in Fig. 3a. As the Q[8] is gradually added, the absorbence of BPE decreases more significantly. This indicates a high binding affinity of Q[8] for BPE. Fig. 3b shows that the 1:2 (host-guest) binding model based on the molar ratio approach closely fits the binding interaction between Q[8] and BPE. Further confirmation that Q[8] forms a stable inclusion complex with BPE with a 1:2 stoichiometry is provided by the continuously varying Job's plot (Fig. S2 in the supplementary material).

The fluorescence spectrum of BPE also changed significantly after the addition of Q[8], as shown in Fig. 4. We know that the guest has no intrinsic fluorescence in aqueous solution, but with the gradual addition of Q[8], the aqueous fluorescence intensity of the guest was somewhat enhanced. This is due to the formation of a 1:2 host-guest inclusion complex, in which the Q[8] host provides the guest with a hydrophobic microenvironment.

3.3. Isothermal titration calorimetry (ITC)

To better understand the properties of the host-guest complex formed on interaction of Q[8] with BPE, isothermal titration calorimetry (ITC) experiments were performed in neutral aqueous solution at ambient temperature (Fig. 5). Both enthalpy and entropy values (ΔH= -29.14 kJ·mol$_{-1}$, $T\Delta S$= 5.40 kJ·mol$_{-1}$, ΔG= -34.54 kJ·mol$_{-1}$) contribute to the formation of the complex as shown in Fig. 5. Reasons include ionic dipole interactions between positively charged guest nitrogen atoms and Q[8] host oxygen atoms, and van der Waals interactions between the guest surface and Q[8] host inner wall, which provide a favourable enthalpy for host-host complexation. Alternatively, an important factor in the increase in entropy may be due to the removal of water molecules from the cavities and portals of the Q[8] and the solvation shell of the BPE. The large binding constant of $(3.67 \pm 0.2) \times 10^5$ M^{-2} for Q[8] and the BPE is derived from the van't Hoff equation ($\ln K = -\Delta H/RT + \Delta S/R$) as well as the enthalpy and entropy values, which were also evaluated by considering the following complexation equilibria $2[BPE]+\{Q[8]\} \rightleftharpoons \{[BPE]_2@Q[8]\}$, $K=\{[BPE]_2@Q[8]\}/\{[BPE]^2\{Q[8]\}\}$ [51].

3.4. Crystal structure of the complex

X-ray diffraction has been used to study the binding behaviour of Q[8] to the guest 1,2-bis(4-pyridyl)ethylene in the solid state. Many attempts were made to form suitable crystal samples and here we present the crystal structure of the host-guest complex $[(C_{48}H_{48}N_{32}O_{16})@2(C_{12}H_{12}N_2)4(Cl)]$. The crystal structure determination revealed that the complex crystallises in an orthorhombic crystal system with the centrosymmetric space group *Pbca*. There is essentially no coherent X-ray scattering beyond about 0.95 Å and no data were used for the refinement beyond this point. The components of the structure were clearly visible using data to 0.95 Å; the SI contains a plot (Fig. S3) showing electron density around the guest molecule which highlights the positions of hydrogen atoms.

As shown in Fig. 6, the guest 1,2-bis(4-pyridyl)ethylene is partially encapsulated by the cavity of the Q[8], which is consistent with the observations using ^{1}H NMR spectroscopy in aqueous solution.

It is clear that the encapsulated guest 1,2-bis(4-pyridyl)ethylene forms a series of hydrogen bonds with the Q[8] (Fig. 7a): the hydrogen bonding interactions between the carbon atom on the pyridyl group and the portal oxygen atom of the Q[8] have a distance of 2.589 Å for C(35)-H(35)…O(1), 2.822 Å for C(35)-H(35)…O(8), 2. 451 Å for C(36)-H(36)…O(6) and 2.899 Å for C(36)-H(36)…O(7). In addition, interactions between adjacent Q[8] molecules were found (Fig. 7b) for C(19)-H(19A)…O(7) for 2.776 Å, C(18)-H(18)…O(7) for 2.635 Å, C(16)-H(16)…O(6) for 2.498 Å and C(13)-H(13A)…O(6) at a distance of 2.462 Å.

In addition, Fig. 8a shows that the encapsulated guest 1,2-bis(4-pyridyl)ethylene also has a large number of hydrogen bonds with the adjacent host Q[8]: the hydrogen on the protonated N atom of the pyridyl group interacts with the portal carbonyl oxygen atom of the adjacent Q[8] in a hydrogen bonding interaction with a N(17)-H(17)…O(3) distance of 2.039 Å and an N(17)-H(17)…O(4) distance of 2.363 Å. Moreover, the hydrogen bonding interaction between Q[8] and the free Cl^- atom has a C(19)-H(19B)…Cl(2) distance of 2.982 Å. Meanwhile, in Fig. 8b, it can be seen there is a hydrogen bonding interaction between the H atom on the C atom attached to the N atom on the pyridine ring of the guest 1,2-bis(4-pyridyl)ethylene and the carbonyl oxygen atom of the Q[8] host, as shown by the C(29)-H(29)…O(3) at a distance of 2.619 Å and C(25)-H(25).. .O(4) distance of 2.332 Å. The large number of hydrogen bonding interactions present here contribute to the formation of the stable inclusion complex.

Squeeze reveals two pockets of electron density associated with disordered solvent in the structure. These are contained within two

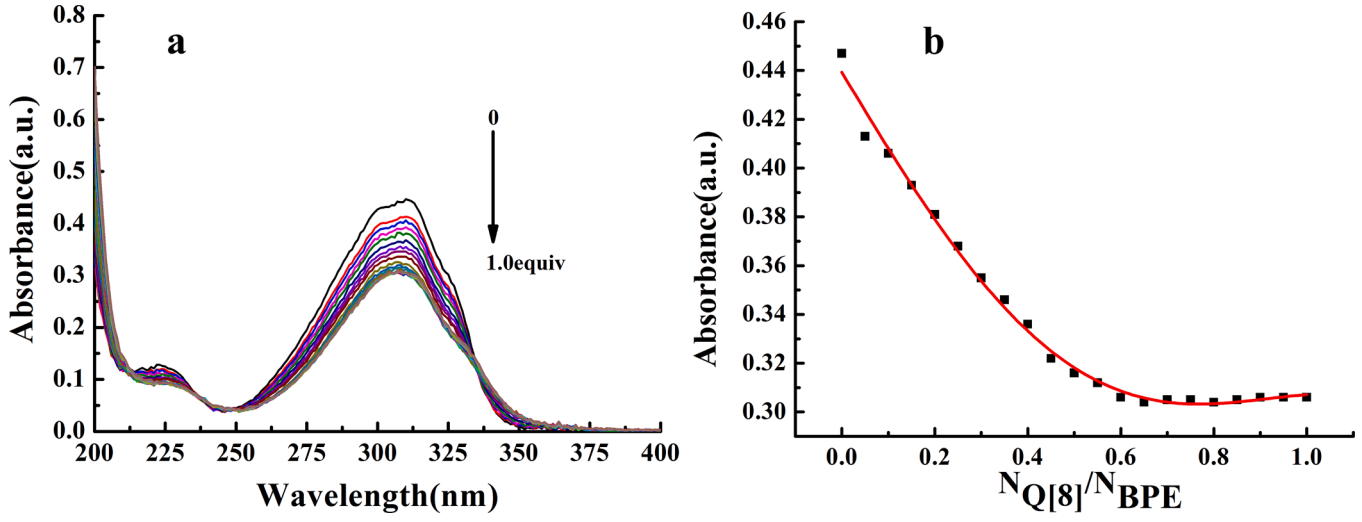

Fig. 3. (a) UV–vis titration of BPE (2×10^{-5} mol·L^{-1}) on increasing concentrations of Q[8]; (b) The molar ratio plot of the absorbence data of $NQ[8]/N_{BPE}$.

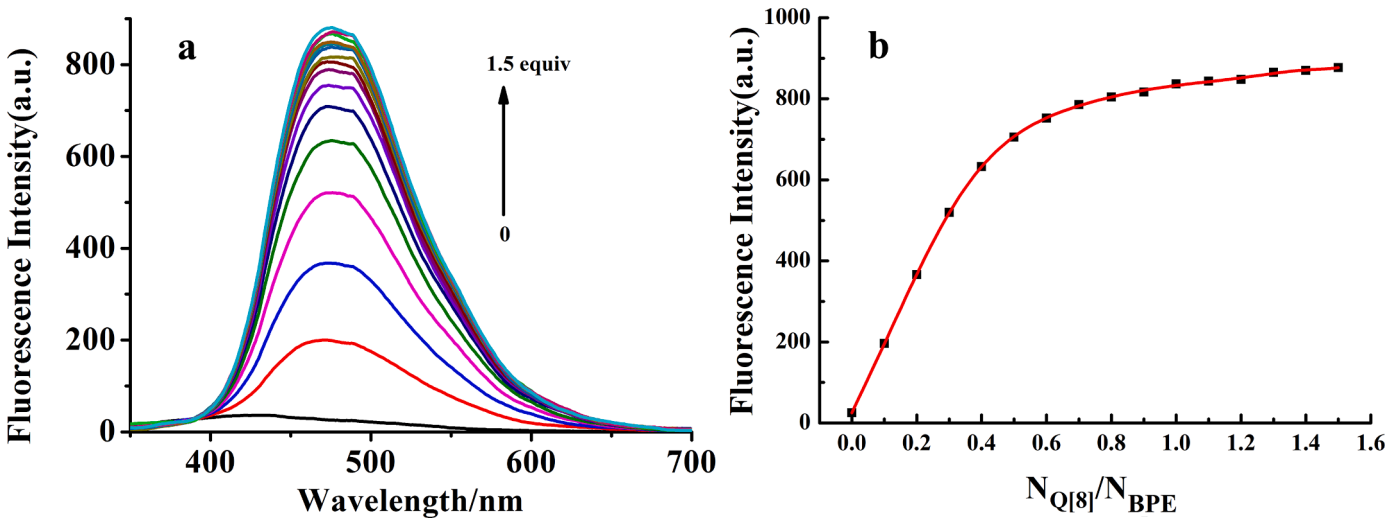

Fig. 4. (a) Fluorescence titration of BPE (2×10^{-5} mol·L^{-1}) on increasing concentrations of Q[8]; (b) A plot of fluorescence intensity, at a wavelength of 478 nm, as a function of $NQ[8]/N_{BPE}$.

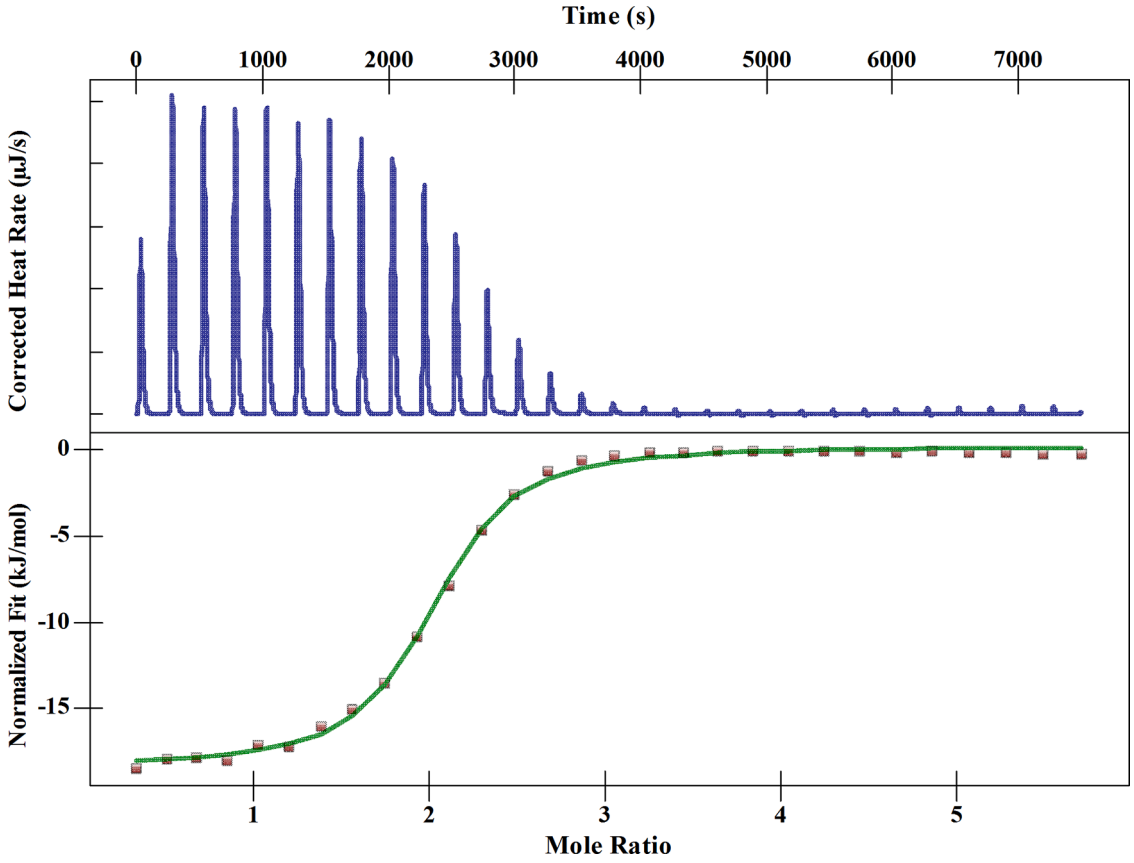

Fig. 5. ITC profile of host Q[8] with guest BPE at 298.15 K.

voids of volume about 2260 Å^3, each corresponding to about 19 % of the cell volume in total. The total volume of disordered solvent is thus around 38% of the crystal volume. Each void corresponds to around 913 electrons, consistent with around 90 water molecules (45 H_2O per asymmetric unit). Disordered water corresponds to approximately one half of the electron density in this crystal. The structure should be formulated as $[(C_{48}H_{48}N_{32}O_{16})@2(C_{12}H_{12}N_2)4(Cl)]\cdot90H_2O$.

3.5. *Fluorescence enhancing of Q[8]/BPE by pymetrozine*

In aqueous solution, the guest BPE shows no intrinsic fluorescence, as mentioned above. However, the resulting host-guest complex shows a weaker fluorescence enhancement when BPE interacts with Q[8]. Fluorescence measurements were performed to determine whether this BPE_2@Q[8] complex could be used to detect common insecticides. Interestingly, when pymetrozine (1×10^{-4} mol·L^{-1}) was added to the 1:2 inclusion complex of Q[8] with BPE (2×10^{-5} mol·L^{-1}), the fluorescence

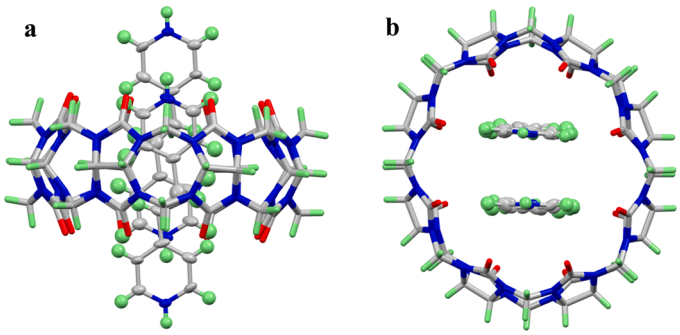

Fig. 6. X-ray crystal structure of the inclusion complex 1 (a) side view; (b) top view.

properties of the inclusion complex BPE_2@Q[8] appeared to change dramatically and a further enhancement of fluorescence was observed. However, the addition of 10 other pesticides (1×10^{-4} mol·L^{-1}) (metalaxyl, tricyclazole, pyroquilon, dodine, paraquat, pyrimethanil, dinotefuran, thiamethoxam, acetamiprid, metoxazon) did not result in any significant fluorescence enhancement (Fig. 9). These observations suggest that the pymetrozine can be selectively detected in aqueous solutions using the BPE_2@Q[8] system.

3.6. *Effect of pymetrozine concentration on the fluorescence intensity of the Q[8]/BPE complex*

The effect of different concentrations of pymetrozine on the fluorescence intensity of the complex BPE_2@Q[8] was also investigated. As shown in Fig. 10a, the fluorescence intensity of the inclusion complex BPE_2@Q[8] gradually increased on increasing the concentration of pymetrozine, while Fig. 7b shows the corresponding fluorescence intensity of the inclusion complex BPE_2@Q[8] when the concentration of pymetrozine was 0–2.0×10^{-5} mol·L^{-1}.

The value of fluorescence intensity change (ΔI) showed a good linear relationship with pymetrozine concentration over a range of concentrations, as shown in Figure S4 in the supplementary material. The linear range was 0–2×10^{-5} mol·L^{-1}, and the linear regression equation was ΔI=35.4025C+12.6771 (C denotes the concentration (mol·L^{-1}) of pymetrozine) with a correlation coefficient of 0.9903, indicating good linearity. The detection limit (DL) for pymetrozine was calculated as 8.01×10^{-7} M.

3.7. *The response mechanism of the fluorescent enhancing*

The ^{1}H NMR spectrum of pymetrozine bound to the inclusion complex BPE_2@Q[8] was also recorded in order to understand the reaction mechanism of the enhanced fluorescence of the inclusion complex BPE_2@Q[8] upon addition of pymetrozine. The results show that the proton peaks H1, H2, H3 of the pymetrozine move to higher field and the proton peaks H4, H5, H6, H7 move to lower fields relative to free pymetrozine, suggesting that the methyl group of the pymetrozine and a portion of its attached ring are encapsulated within the cavity of the Q[8] (Fig. 11). These observations are consistent with the replacement of an encapsulated BPE molecule by a pymetrozine molecule. Thus, BPE and pymetrozine are simultaneously bound within the lumen of Q[8], forming a 1:1:1 ternary inclusion complex. In other words, a certain percentage of the BPE molecule is extruded from the Q[8] cavity and replaced by the pymetrozine molecule.

In the present study, the large Q[8] cavity can accommodate 2.0 equiv. of BPE, forming the 1:2 host-guest inclusion complex BPE_2@Q[8]. The protection invoked by the Q[8] host leads to an enhancement of the fluorescence intensity of the BPE. When pymetrozine was added to the host-guest system of BPE_2@Q[8], the pymetrozine competed for

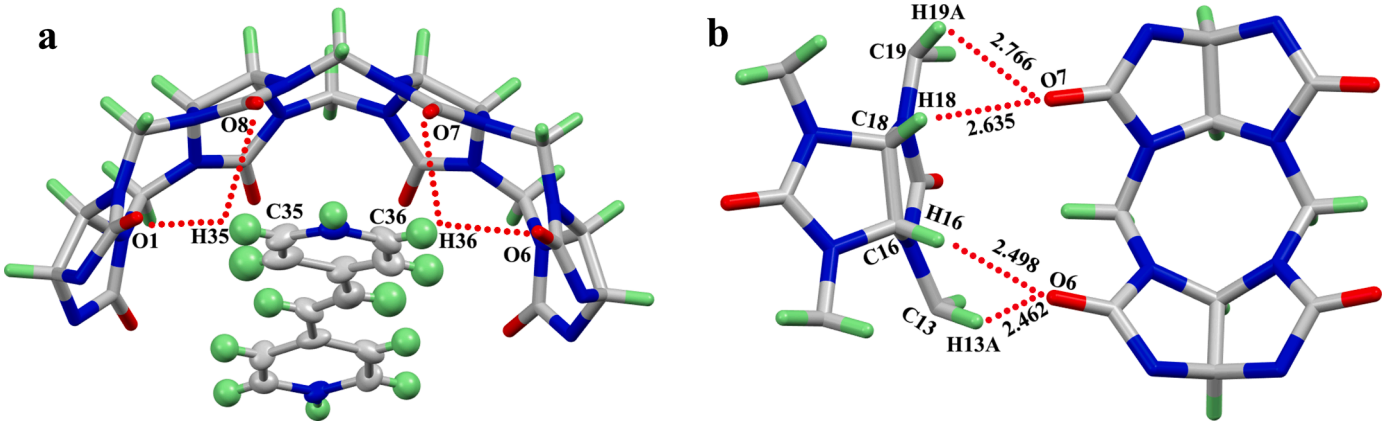

Fig. 7. Ball-and-stick representation of the compound showing guest molecules encapsulated into the Q[8] host, generating an inclusion complex. Solvate water molecules are omitted for clarity; only one guest molecule is shown here. C = light grey, O = red, N = blue and H = light green. (a) Hydrogen bonding interactions between the BPE and the Q[8]; (b)interactions between adjacent Q[8] molecules.

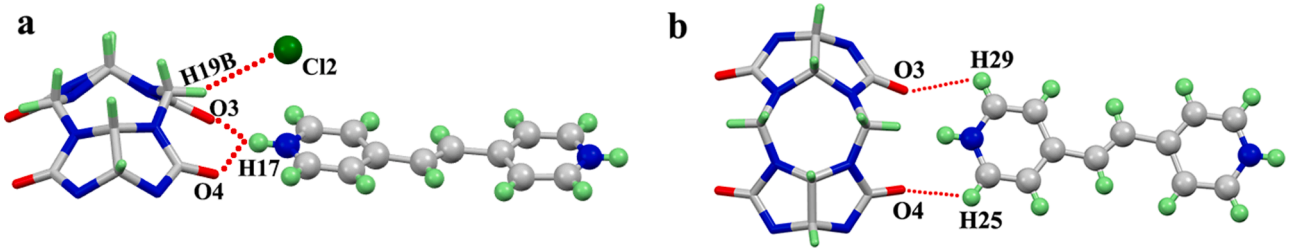

Fig. 8. (a) Hydrogen bonding interactions between the guest BPE and the adjacent Q[8] as well as the free chloride ion; (b) Hydrogen bonding interactions between the guest BPE and the adjacent Q[8] . C = light grey, O = red, Cl= green, N = blue and H = light green.

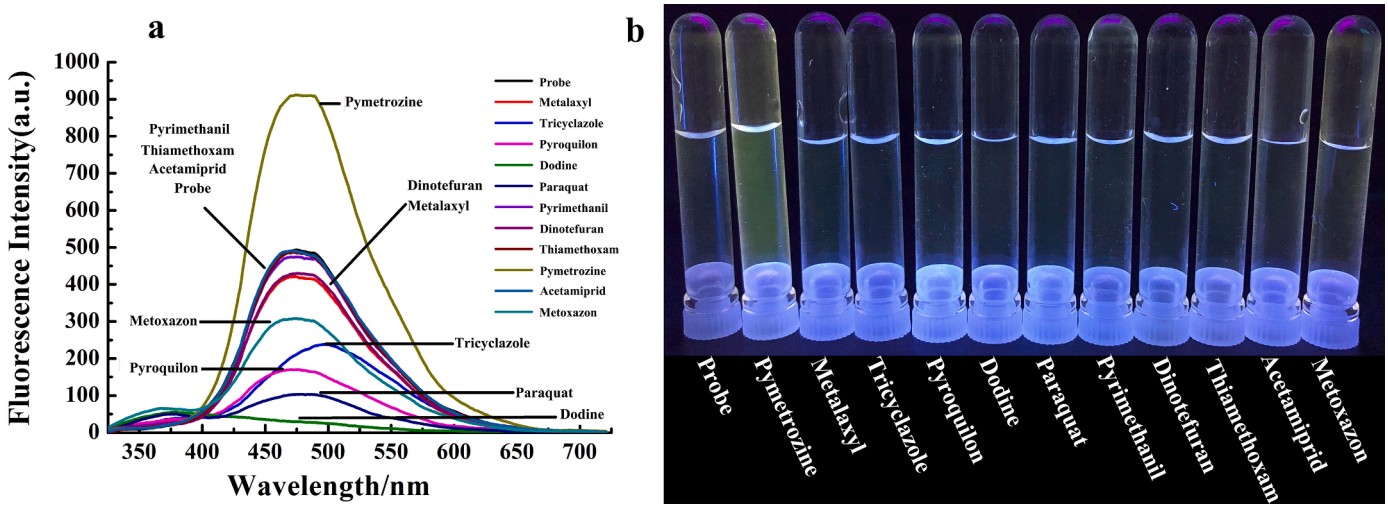

Fig. 9. (a) The fluorescence spectra of Q[8]/BPE with different pesticides in aqueous solution with λ_{ex}= 296 nm; (b) Photographs of different pesticides when added to Q[8]/BPE under exposure to UV light (365 nm).

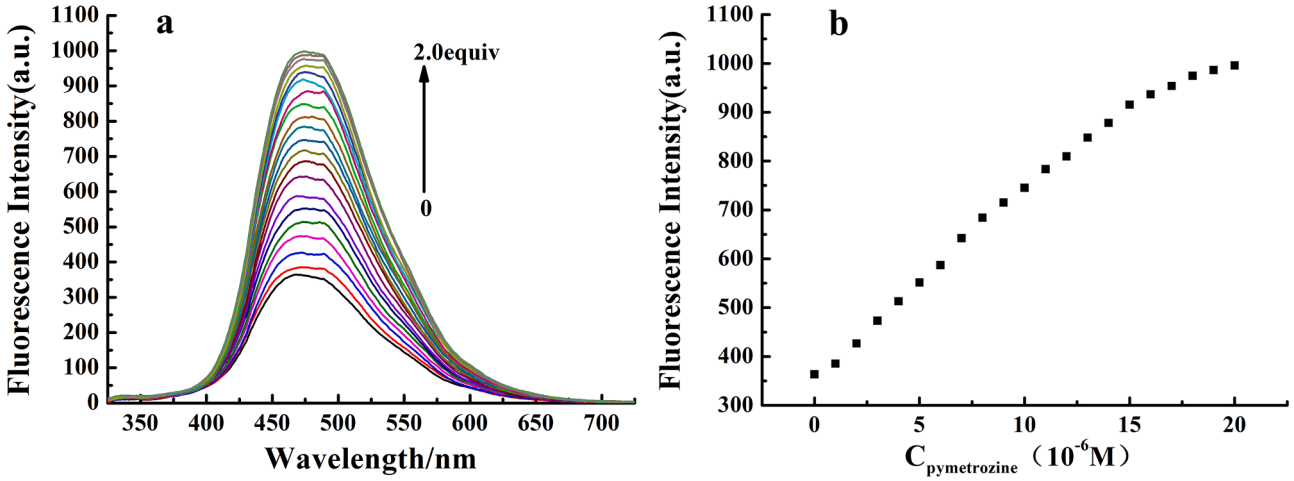

Fig. 10. (a) The fluorescence spectra of Q[8]/BPE at different concentrations of pymetrozine in aqueous solution with λ_{ex}= 296 nm; (b) Corresponding fluorescence intensity of the inclusion complex BPE_2@Q[8] when the concentration of pymetrozine is from 0 to 2.0×10^{-5} mol·L^{-1}.

occupancy of the Q[8] cavity. As observed in the ^{1}H NMR spectra, the result is that the Q[8] cavity accommodated one BPE and one pymetrozine simultaneously. On the basis of the ^{1}H NMR spectra, we speculate that a π...π interaction is formed with the pyridine ring portion of BPE by the methyl ring portion of pymetrozine which is encapsulated by Q[8]. This ternary inclusion complex may be more stable than the BPE_2@Q[8] inclusion complex. The stable ternary inclusion complex resulted in a greater increase in fluorescence intensity. Due to the addition of pymetrozine, the charge transfer between two BPE molecules bound within the cavity of Q[8] is inhibited. At the same time, the formation of a 1:1:1 ternary complex further inhibits the intramolecular rotation of the BPE molecule, so as to increase the fluorescence of the pymetrozine@BPE @Q[8] system. For the other 9 pesticides tested, no enhancement of fluorescence was observed.

4. Conclusions

This paper investigates the binding properties of Q[8] with BPE in aqueous solution by various experimental methods. It was confirmed that the guest BPE can be encapsulated in the cavity of the host Q[8] to form a stable 1:2 host-guest inclusion complex, and that the inclusion complex BPE_2@Q[8] exhibits low intensity fluorescence in aqueous solution. Interestingly, enhanced fluorescence was observed following the addition of the pesticide pymetrozine. At the same time, no significant enhancement of fluorescence was observed after the addition of 10 other pesticides under the same conditions. Thus, a fluorescence probe based on Q[8] and BPE was developed, and this probe is capable of detecting pymetrozine.

Compliance with Ethical Standards

Ethical Approval

This article does not contain any studies with human and animal subjects.

Supplementary material

Structural formulae of the 10 pesticides; Continuous variation Job's plot for Q[8] and the guest on the basis of UV–vis titration spectra; Corresponding plots of fluorescence intensity *versus* pymetrozine concentration. Plot showing electron density around the guest molecule which highlights the positions of hydrogen atoms.

Supplementary crystallographic **material**

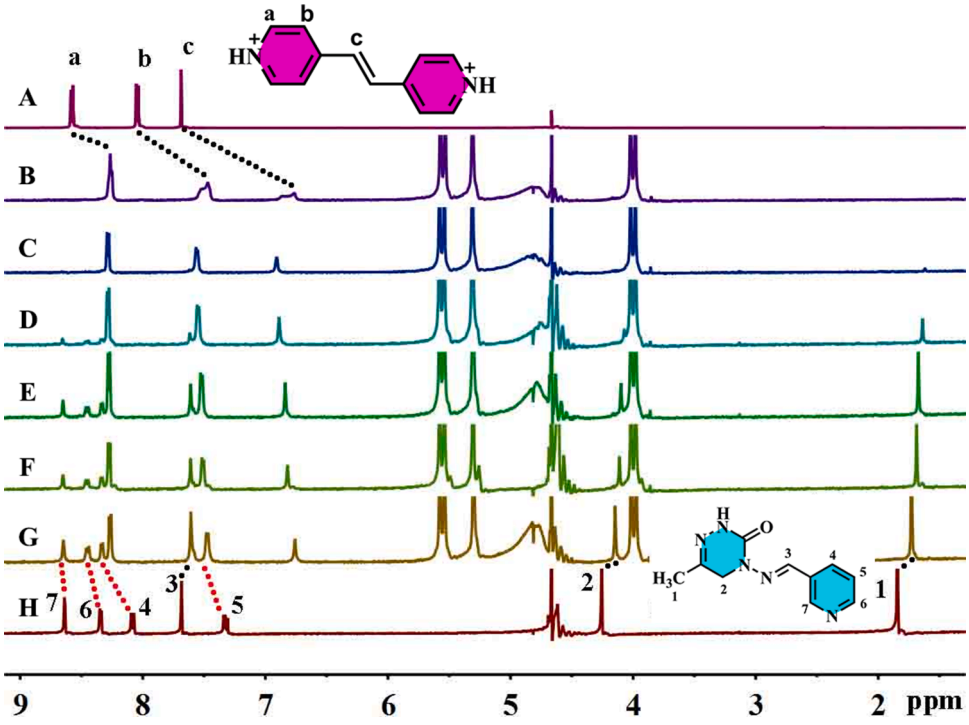

Fig. 11. 1H NMR spectra of BPE (2.0 mmol/L) (A) in the absence of Q[8]; (B) with 0.51 equiv. of Q[8]; (C) with 0.21 equiv. of pymetrozine; (D) with 0.40 equiv. of pymetrozine; (E) 0.61 equiv. of pymetrozine; (F) 0.81 equiv. of pymetrozine; (G) 1.02 equiv. of pymetrozine; (H) neat pymetrozine in D_2O at 20 ℃.

CCDC 2243977 contains the supplementary crystallographic data for this paper. These data can be obtained free of charge via http://www.ccdc.cam.ac.uk/conts/retrieving.html (or from the Cambridge Crystallographic Data Centre, 12, Union Road, Cambridge CB2 1EZ, UK; fax: +44 1223 336033).

CRediT authorship contribution statement

Pei-Hui Shan: Formal analysis, Investigation, Methodology, Data curation, Validation, Writing – original draft. **Ding-Wu Pan:** Validation, Resources, Supervision. **Li-Xia Chen:** Formal analysis, Data curation, Methodology, Project administration, Resources, Supervision, Validation, Visualization. **Timothy J. Prior:** Formal analysis. **Carl Redshaw:** Validation, Writing – review & editing. **Zhu Tao:** Data curation, Validation. **Xin Xiao:** Funding acquisition, Investigation, Data curation, Resources, Visualization, Writing – original draft, Writing – review & editing.

Declaration of Competing Interest

Pei-Hui Shan declares that he has no conflict of interest. Din-Wu Pan declares that he has no conflict of interest. Zhu Tao declares that he has no conflict of interest. Xin Xiao declares that he has no conflict of interest. Timothy J. Prior declares that he has no conflict of interest. Carl Redshaw declares that he has no conflict of interest.

Data availability

Data will be made available on request.

Acknowledgments

We acknowledge the support of Guizhou Provincial Science and Technology Projects (No: ZK [2023] General 040). CR thanks the EPSRC for an Overseas Travel Grant (EP/R023816/1).

Supplementary materials

Supplementary material associated with this article can be found, in the online version, at doi:10.1016/j.molstruc.2023.136418.

References

[1] E. Masson, X.X. Ling, R. Joseph, L. Kyeremeh-Mensah, X.Y. Lu, Cucurbituril chemistry: a tale of supramolecular success, RSC Adv. 2 (2012) 1213–1247.
[2] X.L. Ni, X. Xiao, H. Cong, L.L. Liang, K. Chen, X.J. Cheng, N.N. Ji, Q.J. Zhu, S. F. Xue, Z. Tao, Cucurbit[*n*]uril-based coordination chemistry: from simple coordination complexes to novel poly-dimensional coordination polymers, Chem. Soc. Rev. 42 (2013) 9480–9508.
[3] A.E. Kaifer, Toward Reversible Control of Cucurbit[*n*]uril Complexes, Acc. Chem. Res. 47 (2014) 2160–2167.
[4] M.-S. Li, M. Quan, X.-R. Yang, W. Jiang, Cucurbit[*n*]urils (n = 7, 8) can strongly bind neutral hydrophilic molecules in water, Sci. China Chem. 65 (9) (2022) 1733–1740.
[5] D. Yang, X.N. Yang, M. Liu, L.X. Chen, Q. Li, H. Cong, Z. Tao, X. Xiao, Cucurbit[5] uril-based porous polymer material for removing organic micropollutants in water. Micropor. Mesopor. Mat. 2022, 341, 112023.
[6] X.-L. Ni, Y.-Q. Zhang, Q.-J. Zhu, S.-F. Xue, Z. Tao, Crystal structures of host–guest complexes of meta-tricyclohexyl cucurbit[6]uril with small organic molecules, J. Mol. Struct. 876 (1-3) (2008) 322–327.
[7] D. Yang, M. Liu, X. Xiao, Z. Tao, C. Redshaw, Polymeric self-assembled cucurbit[*n*] urils: Synthesis, structures and applications, Coord. Chem. Rev. 434 (2021), 213733.
[8] R.H. Gao, Y. Huang, K. Chen, Z. Tao, Cucurbit[*n*]uril/metal ion complex-based frameworks and their potential applications, Coord. Chem. Rev. 437 (2021), 213741.
[9] F.F. Shen, J.L. Zhao, K. Chen, Z.Y. Hua, M.D. Chen, Y.Q. Zhang, Q.J. Zhu, Z. Tao, Supramolecular coordination assemblies of a symmetrical octamethyl-substituted cucurbituril with alkali metal ions based on the outer-surface interactions of cucurbit[*n*]urils, CrystEngComm 19 (18) (2017) 2464–2474.
[10] R.H. Gao, L.X. Chen, K. Chen, Z. Tao, X. Xiao, Development of hydroxylated cucurbit[n]urils, their derivatives and potential applications, Coord. Chem. Rev. 348 (2017) 1–24.
[11] W.-T. Xu, Y. Luo, W.-W. Zhao, M. Liu, G.-Y. Luo, Y. Fan, R.-L. Lin, Z. Tao, X. Xiao, J.-X. Liu, Detecting pesticide dodine by displacement of fluorescent acridine from cucurbit[10]uril macrocycle, J. Agric. Food Chem. 69 (2021) 584–591.
[12] Z. Hirani, H.F. Taylor, E.F. Babcock, A.T. Bockus, C.D. Varnado, C.W. Bielawski, A. R. Urbach, Molecular recognition of methionine-terminated peptides by cucurbit [8]uril, J. Am. Chem. Soc. 140 (38) (2018) 12263–12269.

[13] L.C. Smith, D.G. Leach, B.E. Blaylock, O.A. Ali, A.R. Urbach, Sequence-specific, nanomolar peptide binding via cucurbit[8]uril-induced folding and inclusion of neighboring side chains, J. Am. Chem. Soc. 137 (10) (2015) 3663–3669.
[14] G.Y. Guo, Q. Tang, Y. Huang, Z. Tao, S.F. Xue, Q.J. Zhu, Influences on shift of pKa, solubility and antifungal activity offuberidazole by inclusion complexation with cucurbit[*n*]urils, Chin. J. Org. Chem. 34 (11) (2014) 2317–2323.
[15] W. Zhang, Y. Luo, X.-N. Ni, Z. Tao, X. Xiao, Two-step, sequential, efficient, artificial light-harvesting systems based on twisted cucurbit[14]uril for manufacturing white light emission materials, Chem. Eng. J. 446 (2022), 136954.
[16] P.h. Shan, J.h. Hu, M. Liu, Z. Tao, X. Xiao, C. Redshaw, Progress in host-guest macrocycle/pesticide research: recognition, detection, release and application, Coord. Chem. Rev. 467 (2022), 214580.
[17] Z. Hirani, H.F. Taylor, E.F. Babcock, A.T. Bockus, C.D. Varnado Jr., C.W. Bielawski, A.R. Urbach, Molecular recognition of methionine-terminated peptides by cucurbit [8]uril, J. Am. Chem. Soc. 140 (38) (2018) 12263–12269.
[18] J. Liu, C.S.Y. Tan, O.A. Scherman, Dynamic interfacial adhesion through cucurbit [n]uril molecular recognition, Angew. Chem. Int. Ed. 57 (29) (2018) 8854–8858.
[19] X. Zhang, Y. Du, R. Feng, X. Ren, T. Wu, Y. Jia, N. Zhang, F. Li, Q. Wei, H. Ju, An electrochemiluminescence insulin sensing platform based on the molecular recognition properties of cucurbit[7]uril, Biosens. Bioelectron. 227 (2023), 115170.
[20] B.H. Xiao, S.H. He, M.J. Sun, J.H. Zhou, Z.Y. Wang, Y.C. Li, S.M. Liu, W.M. Nau, S. Chang, Dynamic interconversions of single molecules probed by recognition tunneling at cucurbit[7]uril-functionalized supramolecular junctions, Angew. Chem. Int. Ed. 61 (26) (2022), e202203830.
[21] H. Chen, Y.Y. Chen, H. Wu, J.F. Xu, Z.W. Sun, X. Zhang, Supramolecular polymeric chemotherapy based on cucurbit[7]uril-PEG copolymer, Biomaterials. 178 (2018) 697–705.
[22] W. Zhang, Y. Luo, J. Zhao, C. Zhang, X.L. Ni, Z. Tao, X. Xiao, Controllable fabrication of a supramolecular polymer incorporating twisted cucurbit[14]uril and cucurbit[8]uril via self-sorting, Chinese Chem. Lett. 33 (5) (2022) 2455–2458.
[23] Y. Luo, S.Q. Gan, W. Zhang, M.H. Jia, L.X. Chen, C. Redshaw, Z. Tao, X. Xiao, A new cucurbit[10]uril-based AIE fluorescent supramolecular polymer for cellular imaging, Mater. Chem. Front. 6 (8) (2022) 1021–1025.
[24] Y. Luo, W. Zhang, M.X. Yang, X.H. Feng, C. Redshaw, Q. Li, Z. Tao, X. Xiao, A twisted cucurbit[14]uril-based fluorescent supramolecular polymer mediated by metal ion, Macromolecules 55 (5) (2022) 1642–1646.
[25] J. Liu, O.A. Scherman, Cucurbit[*n*]uril supramolecular hydrogel networks as tough and healable adhesives, Adv. Funct. Mater. 28 (21) (2018), 1800848.
[26] C.S.Y. Tan, J. Liu, A.S. Groombridge, S.J. Barrow, C.A. Dreiss, O.A. Scherman, Controlling Spatiotemporal Mechanics of Supramolecular Hydrogel Networks with Highly Branched Cucurbit[8]uril Polyrotaxanes, Adv. Funct. Mater. 28 (7) (2018), 1702994.
[27] M. Liu, L.X. Chen, P.H. Shan, C.J. Lian, Z.H. Zhang, Y.Q. Zhang, Z. Tao, X. Xiao, Pyridine detection using supramolecular organic frameworks incorporating cucurbit[10]uril, ACS Appl. Mater. Inter. 13 (6) (2021) 7434–7442.
[28] Y.Q. Yao, Y.J. Zhang, C. Huang, Q.J. Zhu, Z. Tao, X.L. Ni, G. Wei, Cucurbit[10]uril-based smart supramolecular organic frameworks in selective isolation of metal cations, Chem. Mater. 29 (13) (2017) 5468–5472.
[29] T.T. Zhang, X.N. Yang, J.H. Hu, Y. Luo, H.J. Liu, Z. Tao, X. Xiao, C. Redshaw, New dual-mode orthogonal tunable fluorescence systems based on cucurbit[8]uril: white light, 3D printing, and anti-counterfeit applications, Chem. Eng. J. 452 (2023), 138960.
[30] Y. Huang, R.H. Gao, M. Liu, L.X. Chen, X.L. Ni, X. Xiao, H. Cong, Q.J. Zhu, K. Chen, Z. Tao, Cucurbit[*n*]uril-based supramolecular frameworks assembled through outer-surface interactions, Angew. Chem. Int. Ed. 60 (28) (2021) 15166–15191.
[31] Y.W. Li, C.C. Yan, Q.F. Li, L.P. Cao, Successive construction of cucurbit[8]uril-based covalent organic frameworks from a supramolecular organic framework through photochemical reactions in water, Sci. China Chem. 65 (7) (2022) 1279–1285.
[32] M. Liu, R. Cen, J. Li, Q. Li, Z. Tao, X. Xiao, L. Isaacs, Double-cavity nor-seco-cucurbit[10]uril enables efficient and rapid separation of pyridine from mixtures of toluene, benzene, and pyridine, Angew. Chem. Int. Ed. 61 (2022), e202207209.
[33] T.C. He, X.C. Hu, S.M. Liu, A high-affinity and removable iminium dication guest for recycling of cucurbit[7]uril materials. Org. Lett. 2023, 25(1), 246–250.
[34] T. Goel, N. Barooah, M.B. Mallia, A.C. Bhasikuttan, J. Mohanty, Recognition-mediated cucurbit[7]uril-heptamolybdate hybrid material: a facile supramolecular strategy for (99 m)Tc separation, Chem. Commun. 52 (45) (2016) 7306–7309.
[35] M. Liu, R. Cen, J.S. Li, Q. Li, Z. Tao, X. Xiao, L. Isaacs, Double-cavity nor-seco-cucurbit[10]uril enables efficient and rapid separation of pyridine from mixtures of toluene, benzene, and pyridine, Angew. Chem. Int. Ed. 61 (35) (2022).
[36] P. Bortolus, S. Monti, Photochemistry in Cyclodextrin Cavities, in: D.C. Neckers, D. H. Volman, G. Bunau (Eds.), Advances in Photochemistry, Wiley, Hoboken, 1996, 21.
[37] G.H. Wang, Z.P. Xu, Z.G. Chen, W. Niu, Y. Zhou, J.T. Guo, L. Tan, Sequential binding of large molecules to hairy MOFs, Chem. Commun. 49 (2013) 6641–6643.
[38] R. Fernandez de Luis, M.K. Urtiaga, J.L. Mesa, E.S. Larrea, M. Iglesias, T. Rojo, M. I. Arriortua, Thermal response, catalytic activity, and color change of the first hybrid vanadate containing bpe guest molecules, Inorg. Chem. 52 (2013) 2615–2626.
[39] D. Rani, K.K. Bhasin, M. Singh, Non-porous interpenetrating Co-bpe MOF for colorimetric iodide sensing. Dalton Trans. 2021, 50 (38), 13430–13437.
[40] J.I. Poong, H.G. Koo, H.M. Park, S.P. Jang, Y.J. Lee, C. Kim, S.-J. Kim, Y. Kim, Light-induced self-assemblies suitable for photodimerization and their light-induced [2+2] cycloaddition: Light as a control factor of crystal growth, Inorg. Chimica Acta. 376 (1) (2011) 605–611.
[41] A.N. Pârvulescu, G. Marin, K. Suwinska, V.C. Kravtsov, M. Andruh, V. Pârvulescu, V.I. Pârvulescu, A polynuclear complex, {[Cu(bpe)$_2$](NO$_3$)}, with interpenetrated diamondoid networks: synthesis, properties and catalytic behavior, J. Mater. Chem. 15 (39) (2005) 4234–4240.
[42] F. Klongdee, J. Boonmak, S. Youngme, Anion-dependent self-assembly of copper coordination polymers based on pyrazole-3,5-dicarboxylate and 1,2-di(4-pyridyl) ethylene, Dalton Trans. 46 (14) (2017) 4806–4815.
[43] S. Alghool, C. Slebodnick, Tetranuclear dioxomolybdenum (VI) cluster anion, hydrogen bond interaction with 1,2-di(4-pyridyl)ethylene, J. Therm. Anal. Calorim. 124 (2) (2016) 847–855.
[44] F. Llano-Tomé, B. Bazán, M.-K. Urtiaga, G. Barandika, L. Lezama, M.-I. Arriortua, CuII–PDC-bpe frameworks (PDC = 2,5-pyridinedicarboxylate, bpe = 1,2-di(4-pyridyl)ethylene): mapping of herringbone-type structures, CrystEngComm 16 (37) (2014) 8726–8735.
[45] D. Liu, H.-X. Li, Y. Chen, Y. Zhang, J.-P. Lang, Hydrothermal synthesis and structural characterization of two zinc coordination polymers of 1,2-Di(4-pyridyl) ethylene and Benzenedicarboxylate, Chin. J. Chem. 26 (12) (2008) 2173–2178.
[46] R. Rajendran, L. Neelakantan, Recent advances in estimation of Paraquat using various analytical techniques: A review, Results in Chemistry 5 (2023), 100703.
[47] J. Kim, I.S. Jung, S.Y. Kim, E. Lee, J.K. Kang, S. Sakamoto, K. Yamaguchi, K. Kim, Macrocycles within macrocycles: cyclen, cyclam, and their transition metal complexes encapsulated in cucurbit[8]uril, J. Am. Chem. Soc. 122 (2000) 540–541.
[48] G.M. Sheldrick, SHELXT-Integrated space-group and crystal-structure determination, Acta Crystallogr. C Struct. Chem. 71 (2015) 3–8.
[49] O.V. Dolomanov, L.J. Bourhis, R.J. Gildea, J.A. Howard, K.H. Puschmann, OLEX2: a complete structure solution, refinement and analysis program, J. Appl. Cryst. 42 (2009) 339–341.
[50] A.L. Spek, Single-crystal structure validation with the program PLATON, J. Appl. Crystallogr. 36 (2003) 7–13.
[51] J.R. Lakowicz, Principles of Fluorescence Spectroscopy, 3rd Ed., Springer, New York, 2006.